CHAPTER: 02

MODELING AND CONTROLLER DESIGN FOR DFIG BY USING SOF TECHNIQUE

2.1 Wind Turbine Drive Train and Aerodynamics

The principle of a wind turbine is as follows, the aerodynamic power is converted into mechanical power and then electrical power, where the basic concept of DFIG based variable speed wind turbine is described in [114]. The drivetrain has a turbine, gearbox, shafts and other mechanical components of the wind turbine. A multi-mass is two mass models to be used for dynamic studies of wind turbines through DFIG [115]. A simplified aerodynamic model is sufficient when the speed and pitch angle changes on the aerodynamic power during the grid faults. For stability investigation, the drive train system has to be approximated by the at least a two mass-spring as well as damper model while the system response to heavy disturbance [116]. There is a flexible shaft during the turbine, and generator masses are associated.

2.2 Pitch Angle Control System

The "Pitch Control" is a technique to mechanically adjust the blade pitch angle to change the curve of the power coefficient of the turbine [117]. PI control is used to realize the pitch angle, in servomechanism model with time control T_{servo} accounts for the effective response in the pitch angle control system. For the duration of the grid faults how quick the aerodynamic power can be reduced to stop more spending is decided by the rate of change limit.

2.3 Wind Turbine Modeling

In this section, wind turbine model is discussed for optimal operations of the wind turbine at different wind speeds [118]. It must be operated at its maximum power coefficient ($C_{p\ optimum}$ = 0.3 - 0.45), i.e., at a constant tip speed ratio, intended for operation approximately its maximum power coefficient. The aerodynamic power generated by a wind turbine is given as follows.

$$P_{aero} = 0.5\rho A C_p(\lambda,\beta)v^3 \tag{1}$$

Where $C_p(\lambda,\beta)$ can be expressed as [13]:

$$C_p(\lambda,\beta) = c_1\left(\frac{c_2}{\lambda_i} - c_3.\beta - c_4\right).e^{-\frac{c_5}{\lambda_i}} + c_6.\lambda \tag{2}$$

$\frac{1}{\lambda_i} = \frac{1}{\lambda + 0.08\beta} - \frac{0.35}{\beta^3 + 1}$, and the coefficients

c_1= 0.5176, c_2 = 116, c_3= 0.4, c_4 = 5, c_5= 21, c_6= 0.0068 and $\lambda = \frac{\omega_T.R}{v}$

A = Swept area of the blades (=πR^2)

λ = Tip ratio speed,

ω_T = Rotational speed of the rotor,

β = Pitch angle,

R= Radius of the area covered through the blades.

The speed of a wind turbine determines the conversion efficiency from wind energy to mechanical energy, for a given wind velocity, blades geometry, and turbine orientation and brief description about maximum power point tracking (MPPT) is presented.

2.4 An impression on the DFIG

The overview and operating principle of DFIG discuss in this section is mention in [22]. However, the graphical procedure along with a basic diagram to the DFIG with converters is shown in Figure 1 respectively. The AC/DC/AC converter is divided into two components: The rotor side converter (C_{rotor}) as well as the grid side converter (C_{grid}). C_{rotor} and C_{grid} are voltage sourced converters with a common DC link via a capacitor. The grid converter uses a coupling inductor L to connect to the grid. The three-phase rotor winding is connected to the C_{rotor} through slip rings as well as brushes, while the three-phase stator winding is directly connected to the grid.

2.5 Working standard of DFIG

The power captured by the wind turbines is converted into electrical power by the induction generator also it is transmitted to the grid through both the stator as well as rotor windings. The control system generates the control signals to control the active, reactive power as well as currents, the injected frequency compensation to the rotor windings and lastly the DC voltage control of the common coupling link capacitor. The illustrative installation graphical diagram as a wind generator to the DFIG for operation procedure is shown in Figure (2.1).

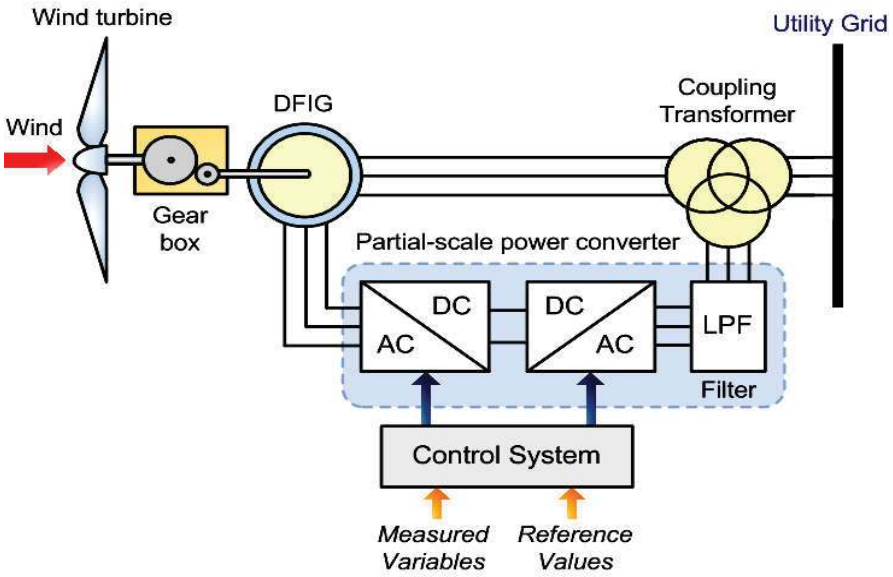

Figure 2.1: DFIG typical installation graphical diagram as a wind generator

Rotor side converter operates as an inverter and stator side connector operates as a rectifier. When rotor moves below the synchronous speed in generating slip power is supplied to the rotor. Whereas in [22], DFIGs have two operating modes which is shown in Figure 1(c) & 1(d) in chapter 1. In (i) mode Nr>Ns, s is –ve, then generator in super-synchronous mode and both stators, as well as rotor windings, convey power to the grid. While in (ii) mode Nr<Ns, s is +ve and the generator in sub-synchronous mode and stator winding provides power to both the grid as well as rotor winding. The mechanical power as well as the stator electric output power is given as below:

$$P_r = T_m * \omega_r \tag{3}$$

$$P_s = T_{em} * \omega_s \tag{4}$$

The mechanical dynamical equations for the lossless generator are described below.

$$J\frac{d\omega_r}{dt} = (T_m - T_{em}) \tag{5}$$

At steady state, the mechanical torque balances the electromagnetic torque substitute on the machine and hence the relations are as follows.

$T_m = T_{em}$ And $P_m = (P_s + P_r)$ it follows that:

$$P_r = (P_m - P_s) = T_m \omega_r - T_{em} \omega_s = -sP_S \tag{6}$$

Here $s = (\omega_s - \omega_r)/\omega_s$ is defined as the slip of the generator in per unit.

2.6 Mathematical Modeling of the DFIG

The mathematical modeling of DFIG is explained clearly in this section [22, 119]. The machine data is available in per unit reactance form because machine and power system parameters are nearly always given in ohms or percent or per unit of base impedance, it is convenient to express the voltage and flux linkage equations regarding reactance's rather than inductances. Thus equilibrium equations of the machine are written as follows. The DFIG equivalent circuit is shown below

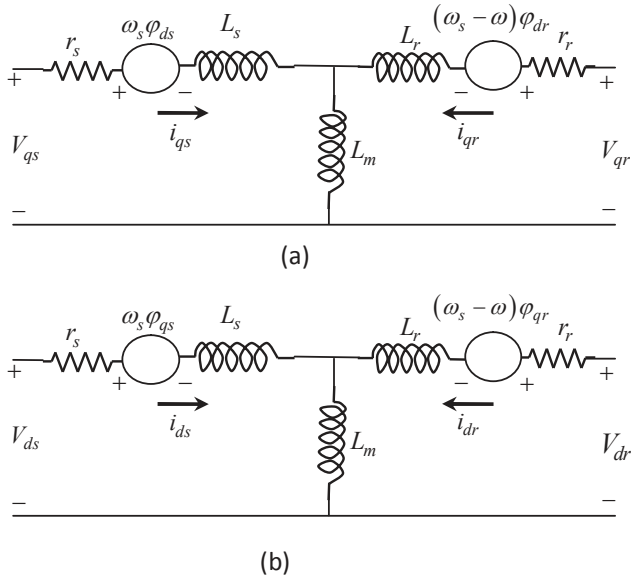

Figure 2.2: DFIG electrical equivalent circuit

$$v_{qs} = r_s i_{qs} + \frac{\omega}{\omega_b}\psi_{ds} + \frac{p}{\omega_b}\psi_{qs} \tag{7}$$

$$v_{ds} = r_s i_{ds} - \frac{\omega}{\omega_b}\psi_{qs} + \frac{p}{\omega_b}\psi_{ds} \tag{8}$$

$$v_{0s} = r_s i_{0s} + \frac{p}{\omega_b}\psi_{ds} \tag{9}$$

$$v'_{qr} = r'_r i'_{qr} + \left(\frac{\omega - \omega_r}{\omega_b}\right)\psi'_{dr} + \frac{p}{\omega_b}\psi'_{qr} \tag{10}$$

$$v'_{dr} = r'_r i'_{dr} - \left(\frac{\omega - \omega_r}{\omega_b}\right)\psi'_{qr} + \frac{p}{\omega_b}\psi'_{dr} \tag{11}$$

$$v'_{0r} = r'_r i'_{0r} + \frac{p}{\omega_b}\psi'_{0r} \tag{12}$$

Here ω_b is the base electrical angular velocity used to calculate the inductive reactance.

And $\omega - \omega_r = \omega_e$ is stator angular speed for steady state operation

Flux linkages per second with the units of volts are presented as follows.

$$\psi_{qs} = X_{ls} i_{qs} + X_M (i_{qs} + i'_{qr}) \tag{13}$$

$$\psi_{ds} = X_{ls} i_{ds} + X_M (i_{ds} + i'_{dr}) \tag{14}$$

$$\psi_{0s} = X_{ls} i_{0s} \tag{15}$$

$$\psi'_{qr} = X'_{lr} i'_{qr} + X_M (i_{qs} + i'_{qr}) \tag{16}$$

$$\psi'_{dr} = X'_{lr} i'_{dr} + X_M (i_{ds} + i''_{dr}) \tag{17}$$

$$\psi'_{0r} = X''_{lr} i''_{0r} \tag{18}$$

In the above equations, the inductive reactance is obtained by multiplying ω_b times inductance.

The voltage equations (7) - (12) are written regarding currents and flux linkages (per second). The currents and flux linkages are interrelated, and both cannot be independent or state variables. In transfer function formulation and computer simulation of induction machines, the desirable results are obtained to express the voltage equations regarding either currents or flux linkages. If currents are selected as independent variables and the flux linkages replaced by the currents, the voltage equation becomes as follows.

$$\begin{bmatrix} v_{qs} \\ v_{ds} \\ v_{0s} \\ v'_{qr} \\ v'_{dr} \\ v'_{0r} \end{bmatrix} = \begin{bmatrix} r_s + \frac{p}{\omega_b} X_{ss} & \frac{\omega}{\omega_b} X_{ss} & 0 & \frac{p}{\omega_b} X_M & \frac{\omega}{\omega_b} X_M & 0 \\ \frac{\omega}{\omega_b} X_{ss} & r_s + \frac{p}{\omega_b} X_{ss} & 0 & \frac{\omega}{\omega_b} X_M & \frac{p}{\omega_b} X_M & 0 \\ 0 & 0 & r_s + \frac{p}{\omega_b} X_{ls} & 0 & 0 & 0 \\ \frac{p}{\omega_b} X_M & \left(\frac{\omega - \omega_r}{\omega_b}\right) X_M & 0 & r'_r + \frac{p}{\omega_b} X'_{rr} & \left(\frac{\omega - \omega_r}{\omega_b}\right) X'_{rr} & 0 \\ -\left(\frac{\omega - \omega_r}{\omega_b}\right) X_M & \frac{p}{\omega_b} X_M & 0 & -\left(\frac{\omega - \omega_r}{\omega_b}\right) X'_{rr} & r'_r + \frac{p}{\omega_b} X'_{rr} & 0 \\ 0 & 0 & 0 & 0 & 0 & r'_r + \frac{p}{\omega_b} X'_{lr} \end{bmatrix} \begin{bmatrix} i_{qs} \\ i_{ds} \\ i_{0s} \\ i'_{qr} \\ i'_{dr} \\ i'_{0r} \end{bmatrix} \tag{19}$$

Where, $X_{SS} = X_{ls} + X_M$ (20)

$$X'_{rr} = X'_{lr} + X_M \tag{21}$$

If $\omega = \omega_b$, the rotating speed of the reference frame is same as 120π rad/s. This reference frame is called asynchronously synchronous reference frame. The air gap flux linkages ψ_{qm} and ψ_{dm} can then be expressed as follows.

$$\psi_{qm} = L_m(i_{qs} + i_{qr}^{'}) \tag{22}$$

$$\psi_{dm} = L_m(i_{ds} + i_{dr}^{'}) \tag{23}$$

The electromagnetic torque T_e can be expressed as follows

$$T_e = \frac{3}{2}\left(\frac{p}{2}\right)\left(\psi_{qm} i_{dr} - \psi_{dm} i_{qr}\right) \tag{24}$$

Where; T_e is the electromagnetic torque for air gap flux linkages (ψ_{qm}, ψ_{dm}) per second and rotor q plus d winding currents ($i_{dr,}$ i_{qr}) respectively [119].

The power loss associated with the stator resistance is small enough to be ignored; therefore the approximation of electromagnetic power can be written as

$$\text{Active power } (P_s) = (v_{ds} i_{qs} + v_{qs} i_{ds}) \tag{25}$$

The reactive power absorbed by the grid or injected into the grid is evaluated by the following equation.

$$Q_s = (v_{qs} i_{ds} - v_{ds} i_{qs}) \tag{26}$$

The electrical torque is illustrated below.

$$T_s = \psi_{dr} i_{qs} - \psi_{qr} i_{ds} \tag{27}$$

Here T_S is the per unit electrical torque and i_{qs}, i_{ds} is the stator q plus d winding current of the machine [119].

Let us suppose that the reference frame is the synchronous reference frame Furthermore all quantities are in per unit value [120] can be further written as follows.

$$\dot{X} = AX + BU \tag{28}$$

Where $X = \begin{bmatrix} i_{qs} \\ i_{ds} \\ i_{0s} \\ i'_{qr} \\ i'_{dr} \\ i'_{0r} \end{bmatrix}$ and $= B \begin{bmatrix} \frac{X_{ss}}{\omega_b} & 0 & 0 & \frac{X_m}{\omega_b} & 0 & 0 \\ 0 & \frac{X_{ss}}{\omega_b} & 0 & 0 & \frac{X_m}{\omega_b} & 0 \\ 0 & 0 & \frac{X_{ls}}{\omega_b} & 0 & 0 & 0 \\ \frac{X_m}{\omega_b} & 0 & 0 & \frac{X'_{rr}}{\omega_b} & 0 & 0 \\ 0 & \frac{X_m}{\omega_b} & 0 & 0 & \frac{X'_{rr}}{\omega_b} & 0 \\ 0 & 0 & 0 & 0 & 0 & 0 \end{bmatrix}^{-1}$

$$A = -B \begin{bmatrix} r_s & \frac{\omega}{\omega_b} X_{ss} & 0 & 0 & \frac{\omega}{\omega_b} X_m & 0 \\ -\frac{\omega}{\omega_b} X_{ss} & r_s & 0 & -\frac{\omega}{\omega_b} X_m & 0 & 0 \\ 0 & 0 & r_s & 0 & 0 & 0 \\ 0 & \frac{\omega-\omega_r}{\omega_b} X_m & 0 & r'_r & \frac{\omega-\omega_r}{\omega_b} X'_{rr} & 0 \\ -\frac{\omega-\omega_r}{\omega_b} X_m & 0 & 0 & \frac{\omega-\omega_r}{\omega_b} X'_{rr} & r'_r & 0 \\ 0 & 0 & 0 & 0 & 0 & r'_r \end{bmatrix} \tag{29}$$

The swing equation of the machine is given as [119]:

$$T_e = 2H\dot{\omega}_r + T_m \tag{30}$$

Where; $H = \frac{1}{2}\left(\frac{2}{P}\right)^2 J \frac{{\omega_b}^2}{P_b}$ (31)

Whereas, differential equations (19) and (30) represent the induction machine with its fifth-order model in balanced operations and sixth order relations for unbalanced operations.

2.7 Voltage Source Converter Controller

A voltage source converter (VSC) is used in DFIG to control the rotor and grid side converter as well as DC link voltage also. The general schematic diagram of a DFIG and Wind Turbine along with VSC Converters with common DC link is as shown in Figure (2.3). The advantage of VSC based converter is that it uses very small power converter on the rotor side. The rotor side converter supplies the compensated current for frequency compensation. Wide variation in the wind speed is taken care of by gear train with adjustable gear ratio. DC VSC control circuitry provides the necessary control signals for both rotor side as well as grid side converters. Further, the control strategy maintains a constant DC voltage of the common link.

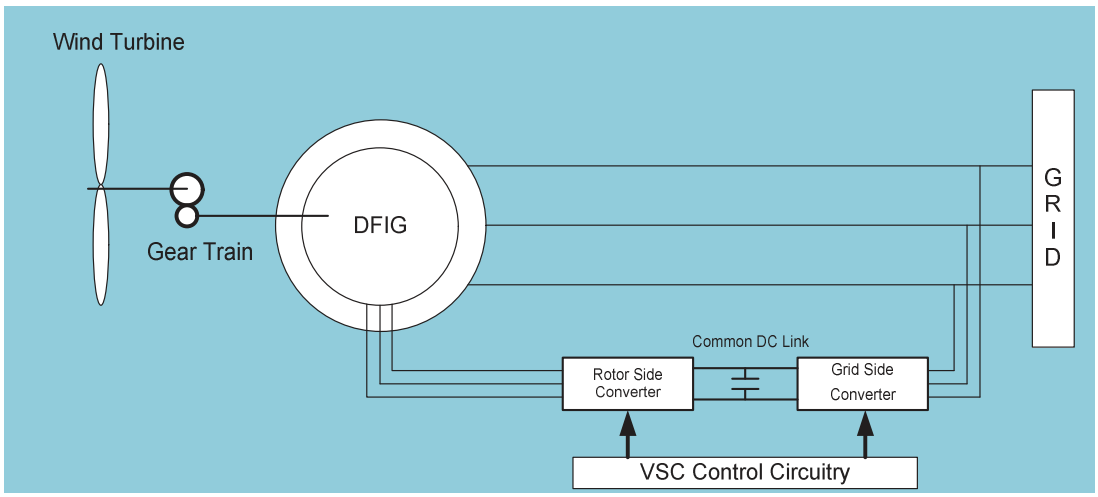

Figure 2.3: The general schematic diagram of a DFIG control

The transfer function of the overall system is obtained either via simple modeling or using the numerical differentiation, by which the controller for the VSC is designed. Component modules of the VSC based common DC link controller are shown in Figure (2.4). P_g^{set} And Q_g^{set} shown in the diagram are the set-point values of the real and reactive power across the terminals of the wind turbine. The power factor can be made unity by letting them Q_g^{set} to zero. In this case, all reactive power to the DFIG is provided via the rotor-side converter. Further, the reactive power set point value can be adjusted to maintain the voltage constant at the turbine terminals [46].

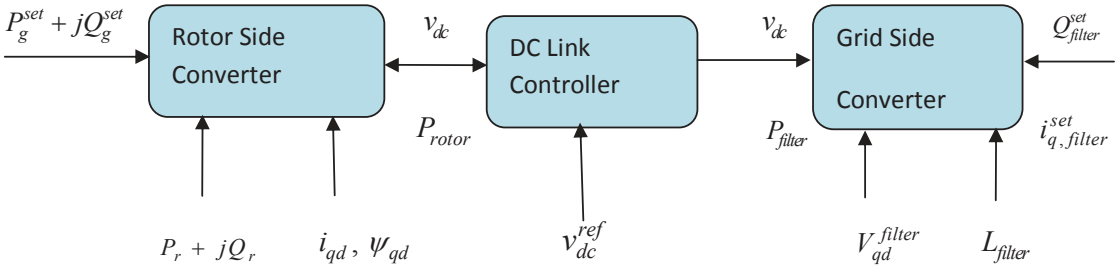

Figure 2.4: Component modules of the VSC based common DC link controller

2.7.1 Simplified System Model

The system was chosen for study for the supervisory control a wind turbine connected to a step-up transformer which is connected to the local load at 1 km away. The point of common coupling at the load side is connected to the utility grid via a 30 km long transmission line [46]. Grid-connected wind turbine system is shown in Figure (2.5).

The supervisory control is used in this chapter to decide the reactive power requirements from the perturbations at the point of common coupling (PCC) to the voltage. On the other hand, the supervisory control scheme is used to regulate the voltage at the specified remote PCC by adjusting the reactive power produced by the individual wind turbines even as taking into

account its operating limits. In general, for the wind farms or even few wind turbines connected to local load and utility grid, it's hard to obtain the analytical model of the overall system.

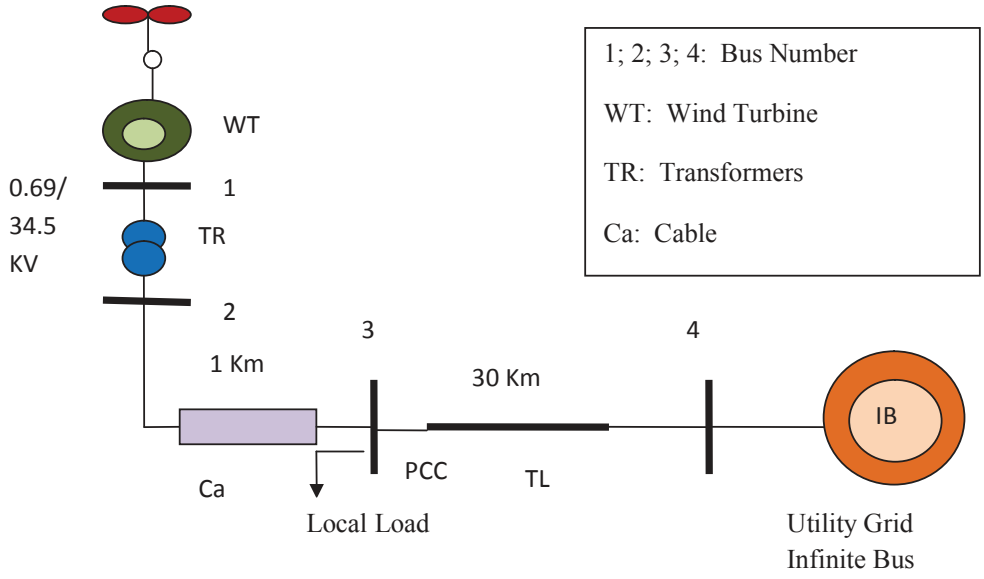

Figure 2.5: Grid connected wind turbine system

However, the numerical differentiation capability of the SIMULINK comes to our rescue, with the help of which a higher order state space model can be derived for SIMULINK models. The obtained reduced model is in a phase variable canonical form which is realized regarding the state variables that are related to the voltage at the PCC (v_{pcc}) and contains proportional and derivative states for zero steady-state error as:

$$\tilde{x} = [\Delta v_{pcc} \quad \Delta \dot{v}_{pcc} \quad \Delta \ddot{v}_{pcc} \quad \Delta \dddot{v}_{pcc}]^T \tag{32}$$

It is imperative to enhance the model with the help of an integrator to reduce the steady-state tracking error zero. This results in enhancement of the state vector as given below.

$$X(t) = [\int_0^\infty (v_{pcc}^{set} - v_{pcc})dt \quad \tilde{x}]^T \tag{33}$$

Thus the overall system along with the integrator used to compensate for variation in the PCC set point voltage and the actual one can be represented in state space form as follows:

$$\dot{x}(t) = Ax(t) + Bu(t) \tag{34}$$

$$\text{Z (t)} = \quad Cx(t) + Du(t) \tag{35}$$

Where A, B, C, D are the augmented system matrices [44]. And also named by as A: is the state matrix; B: is the input matrix; C: is the output matrix, and D is the direct feedthrough matrix; and x is the state vector; u is the input signal vector, and z is output vector.

$$\text{A} = \begin{bmatrix} 0 & -\widetilde{C} \\ 0 & \widetilde{A} \end{bmatrix}, \quad \text{B} = \begin{bmatrix} -\widetilde{D} \\ \widetilde{B} \end{bmatrix}, \; C = \begin{bmatrix} 1 & 0 & 0 & 0 & 0 & 0 \\ 0 & 1 & 0 & 0 & 0 & 0 \end{bmatrix}, \; D = \begin{bmatrix} 0 \\ 0 \\ 0 \end{bmatrix} \tag{33}$$

$\widetilde{A}, \widetilde{B}, \widetilde{C}, \widetilde{D}$, are the system matrices for the system reduced model and is of fifth order. Given below are the state space equations for the simple system under study [44]. The chosen model has been taken from the reference just for the sake of comparison of the results obtained; otherwise model of any order can be obtained via numerical differentiation in Simulink.

$$A = \begin{bmatrix} 0.0092 & 6.89150 & 10.2209 & -1.7963 & 6.09420 & 0 \\ -0.49337 & -10.408 & -54.899 & 6.36430 & -17.017 & 0 \\ 0 & 54.8990 & -52.306 & 13.7505 & -76.688 & 0 \\ 0 & -6.3643 & 13.7505 & -4.7933 & 72.8850 & 0 \\ -0.00318 & -17.017 & 76.6880 & -72.885 & -99.634 & 0 \\ 0 & 0 & 0 & 0 & 0 & 0.01 \end{bmatrix}, \; B = \begin{bmatrix} 0.02820 \\ -6.8915 \\ 10.2209 \\ -1.7963 \\ -6.0942 \\ 0.0001 \end{bmatrix} \tag{36}$$

$$C = \begin{bmatrix} 1 & 0 & 0 & 0 & 0 & 0 \\ 0 & 1 & 0 & 0 & 0 & 0 \end{bmatrix}, \qquad D = \begin{bmatrix} 0 \\ 0 \\ 0 \end{bmatrix} \tag{37}$$

However, the Transfer function of the 6th order reduced model for the DFIG system is presented by [H.S.CO et al]:

$$G(S) = \frac{0.000324s6 - 1.75s5 - 2366s4 + 7.9e6s3 + 7.5e9s2 + 5e12s + 2.18e14}{s6 + 2340s5 + 8.67e6s4 + 4.79e9s3 + 2.7e12s2 + 1.27e14s + 9.6e14} \tag{38}$$

2.7.2 Supervisory Controller Design

The PID controller for the sample system was designed considering the 10% overshoot and more than 60 degrees of phase margin. The Gains of the PID supervisory controller parameters are given in Table1 [44]. However, the study of the DFIG with PI controllers for the internal loops to the DFIG and one PID controller for the supervisory control of the system under revise as proposed in [44]. This model is utilized to design the SOF controller for the proposed system and results are compared with the results in Table2.1.

Table2. 1: Gains of the PID supervisory controller

Parameters	k_i	k_p	k_d
Gains	*6.7122*	0.4635	0.0009

2.8 Static Output Feedback Technique

Various techniques are available in control systems to design PI controller. Among these techniques, static output feedback (SOF) is the one that can be applied to the controller to make the system globally stable.

The focal contribution consists in providing a new sufficient condition to the existence of a SOF gain. Although only sufficient condition has demonstrated an excellent performance compared to the existing results for linear continuous and discrete-time systems. An extension to the H_∞ SOF control problem is also presented [121].

Figure (2.6) shows that input to the PID controller is the error between the setpoint value and the measured value of the plant. Controllers output can be written as follows.

$$u = k_P y_0 + k_I \int y_0 dt + k_d \frac{dy_o}{dt} \tag{39}$$

Where, y_0= e (t), k_P and k_I are controller constants. Equation (39) can be rewritten as follows.

$$u = [\, k_P \;\; k_I \;\; k_D \,]\, [\, y_0 \;\; \int y_0 \;\; \frac{dy_o}{dt} \,]^{\mathrm{T}} \tag{40}$$

Therefore, measured output will be;

$$y = [\, y_0 \;\; \int y_0 \;\; \frac{dy_o}{dt} \,]^{\mathrm{T}} \tag{41}$$

PID controller can be described as follows:

$G_C = [\, k_P \; k_I \; k_D \,]$

Where G_C is gain of the system

Now The PID controller is in closed loop system as shown in Figure (2.6).

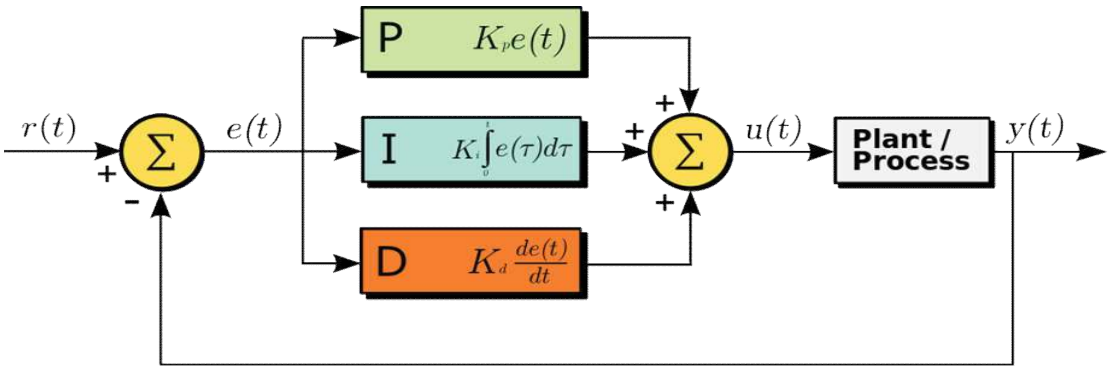

Figure 2.6: PID controller in closed loop system

2.8.1 Controller design using SOF method

Controller design based on SOF method uses a pair of coupled linear matrix inequalities. SOF controller that guarantees the closed-loop system is impulse free and stochastically stable for the tuning of PID controller Considering dynamical singular system defined by following differential-algebraic equation [120],

$$\begin{cases} E(r_1)\dot{x}(t) = A(r_1,t)x(t) + B(r_1,t)u(t), x(0) = x_0 \\ y(t) = C(r_1)x(t) \end{cases} \tag{42}$$

The controller can be given by:

$$u(t) = F(r_1)y(t) = F(r_1)C(r_1)x(t) \tag{43}$$

Where $x(t) \in R^n$ is the state vector, $x_0 \in R^n$ is the initial state, $u(t) \in R^m$ is the control Input, $y(t) \in R^p$ is the output of the system at time t, $\{r, t \geq 0\}$ is the continuous-time Markov process taking values in a finite space $\rho = \{1, 2 \ldots N\}$. Where, $F(i) \in \Re^{m \times p} \forall i \in \rho$ is a design parameter.

Now the nominal system state equation of (42) is as follows

$$E(r_1)\dot{x}(t) = [A(r_1)x(t) + B(r_1)\,\mathrm{u(t)})] \tag{44}$$

Putting controller (43) in the above nominal system state equation; we have,

$$E(r_1)\dot{x}(t) = [A(r_1) + B(r_1)F(r_1)C(r_1)]x(t) \tag{45}$$

$$= A_{cl}(r_1)x(r_1) \tag{46}$$

Whereas $r_1 = i \in \rho$;

With $A_{cl}(i) = A(i) + B(i)F(i)C(i)$ (47)

If system exists a set of nonsingular matrices, $P = (P(1),.....,P(N)), P(i) \in \Re^{n\times n}$ such that the following hold for a given positive scalar ε_p, then the closed loop system is piecewise regular, impulse-free and stochastically stable:

$$\varepsilon_p[P(i) + P^T(i)] \geq E^T(i)P(i) = P^T(i)E(i) \geq 0 \tag{48}$$

$$P^T(i)A_{cl}(i) + A_{cl}{}^T(i)P(i) + \lambda_{ii}E^T(i)P(i) + \Sigma^N{}_{j=1,j\neq i}\,\varepsilon_p\lambda_{ij}[P(j) + P^T(j)] < 0 +$$

$$\Sigma^N{}_{j=1,j\neq i}\,\varepsilon_p\lambda_{ij}[P(j) + P^T(j)] < 0 \tag{49}$$

Then, the second matrix inequality is given by:

$$\begin{aligned} &P^T(i)A(i) + A^T(i)P(i) + P^T(i)B(i)F(i)C(i) + \\ &[P^T(i)B(i)F(i)C(i)]^T + \lambda_{ii}E^T(i)P(i) + \sum_{j=1,j\neq i}^{N}\varepsilon_p\lambda_{ij}[P(j) + P^T(j)] < 0 \end{aligned} \tag{50}$$

To put above inequality into the LMI form let $X(i) = P^{-1}(i)$. Pre-and post-multiply

This inequality respectively by $X^T(i)$ and $X(i)$ give:

$$A(i)X(i) + X^T(i)A^T(i) + B(i)F(i)C(i)X(i) + X^T(i)C^T(i)F^T(i)B^T(i) + \lambda_{ii}X^T(i)E^T(i) + \sum_{j=1, j\neq i}^{N} \varepsilon_p \lambda_{ij} X^T(i)[X^{-1}(j) + X^{-T}(j)]X(i) < 0 \quad (51)$$

Similarly, the first condition can be transformed to:

$$\varepsilon_p \left[X(i) + X^T(i) \right] \geq X^T(i)E^T = EX(i) \geq 0 \quad (52)$$

Using the fact that:

$$X^{-1}(j) + X^{-T}(j) \leq \mathrm{I} + X^{-1}(j)X^{-T}(j) \quad (53)$$

$$= \mathrm{I} + [X^T(j)X(j)]^{-1} \quad (54)$$

Let,

$$Z_i(X) = diag[X^T(1)X(1),....,X^T(i-1)X(i-1), X^T(i+1)X(i+1),....,X^T(N)X(N)] \quad (55)$$

We get,

$$\sum_{j=1, j\neq 1}^{N} \varepsilon_p \lambda_{ij} X^T(i)\left[X^{-1}(j) + X^{-T}(j)\right]X(i) \leq S_i(X)S_i^T(X) + S_i(X)Z_i^{-1}(X)S_i^T(X) \quad (56)$$

Where $S_i(X)$ is defined as follows:

$$S_i(X) = [\sqrt{\varepsilon_p \lambda_{i1}}X^T(i),.....,\sqrt{\varepsilon_p \lambda_{ii-1}}X^T(i),\sqrt{\varepsilon_p \lambda_{ii+1}}X^T(i),.....,\sqrt{\varepsilon_p \lambda_{iN}}X^T(i)] \quad (57)$$

Now, if we assume $F(i) = G(i)Y^{-1}(i)$ and $Y(i)C(i) = C(i)X(i)$ hold for every $i \in \rho$ for some appropriate matrices that we have to determine and using the fact that:

$$X^T(i)X(i) \geq X^T(i) + X(i) - \mathrm{I} \tag{58}$$

We have,

$$\begin{aligned} &A(i)X(i) + X^T(i)A^T(i) + B(i)G(i)C(i) + C^T(i)G^T(i)B^T(i) + \\ &\lambda_{ii}X^T(i)E^T(i) + S_i(X)S_i^T(X) + S_i(X)\mathrm{Z}_i^{-1}(X)S_i^T(X) < 0 \end{aligned} \tag{59}$$

With,

$$\begin{aligned} &Z_i(X) = diag[X^T(1) + X(1) - \mathrm{I}, \ldots., X^T(i-1) + X(i-1) - \mathrm{I}, \\ &X^T(i+1) + X(i+1) - \mathrm{I}, \ldots., X^T(N) + X(N) - \mathrm{I}] \end{aligned} \tag{60}$$

Using the Schur complements gives:

$$\begin{bmatrix} J(i) & S_i(X) & S_i(X) \\ S_i^T(X) & -\mathrm{I} & 0 \\ S_i^T(X) & 0 & -\mathrm{Z}_i(X) \end{bmatrix} < 0 \tag{61}$$

Where,

$$J(i) = A(i)X(i) + X^T(i)A^T(i) + B(i)G(i)C(i) + C^T(i)G^T(i)B^T(i) + \lambda_{ii}X^T(i)E^T(i)$$

Above results can be summarized by the following theorem.

2.8.2 Theorem

Let ε_p be given positive scalar. There exists a static output feedback controller of the form (43) such that the closed-loop system (42) is piecewise regular, impulse free and stochastically stable if there exist a set of nonsingular matrices $X = (X(1), \ldots\ldots., X(N))$ with $X(i) \varepsilon \Re^{n \times n}$ and $Y = (Y(1), \ldots., Y(N))$ with $Y(i) \varepsilon \Re^{p \times p}$, and a set of matrices $G = (G(1), \ldots\ldots G(N))$ with $G(i) \varepsilon \Re^{m \times p}$ such that the next hold for each $i \varepsilon \rho$:

$$\begin{bmatrix} J(i) & S_i(X) & S_i(X) \\ S_i^T(X) & -\mathrm{I} & 0 \\ S_i^T(X) & 0 & -\mathrm{Z}_i(X) \end{bmatrix} < 0 \tag{62}$$

Where,

$$J(i) = A(i)X(i) + X^T(i)A^T(i) + B(i)G(i)C(i) + C^T(i)G^T(i)B^T(i) + \lambda_{ii}X^T(i)E^T(i) \tag{63}$$

$$S_i(X) = [\sqrt{\varepsilon_p\lambda_{i1}}X^T(i), ..., \sqrt{\varepsilon_p\lambda_{ii-1}}X^T(i), \sqrt{\varepsilon_p\lambda_{ii+1}}X^T(i), ..., \sqrt{\varepsilon_p\lambda_{iN}}X^T(i)] \tag{64}$$

$$\begin{aligned} Z_i(X) = diag[&X^T(1) + X(1) - \mathrm{I}, ..., X^T(i-1) + X(i-1) - \mathrm{I}, \\ &X^T(i+1) + X(i+1) - \mathrm{I}, ..., X^T(N) + X(N) - \mathrm{I}] \end{aligned} \tag{65}$$

With following constraints:

$$\begin{cases} \varepsilon_p[X(i) + X^T(i)] \geq E(i)X(i) = X^T(i)E^T(i) \geq 0 \\ Y(i)C(i) = C(i)X(i) \end{cases} \tag{66}$$

The Controller gain is given by $F(i) = G(i)Y^{-1}(i)$ (67)

By entering all the value of the matrices given in the equations (36) and (37) in above optimization problem theorem and solve using LMI Toolbox of MATLAB and we get the Gain of the SOF based controller as given in Table (2.2).

Table 2.2 Gains of the SOF controller

states	k_p	k_i	k_d
Gains	0.0814	4.6647	0.0000

Now the Flowchart for SOF based controller design is given in flowing Figure (2.7). The discussions of the PID gains optimized are determined by using SOF has been presented in the following flow chart which is given below.

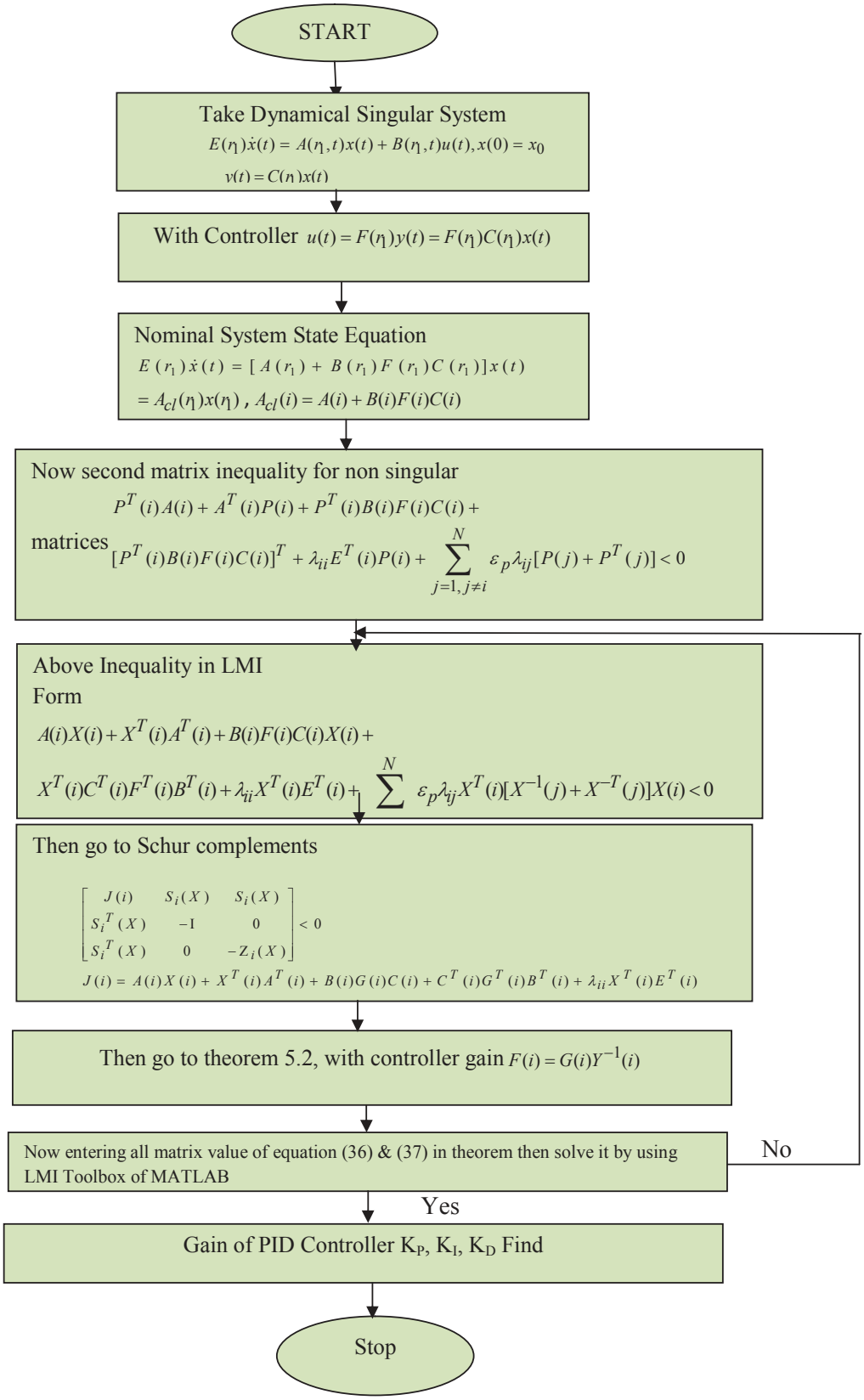

Figure2.7: Flowchart for SOF based controller design

2.9. Simulation and Results

2.9.1 Simulation and Response of the DFIG System

Here a DFIG connected with variable speed wind turbine has been taken from Matlab Simulink. Initially, the DFIG wind farm produces 1.8 MW. This active power corresponds to the maximum wind turbine output power for 10m/s wind speed is merely equal to 1.95 MW minus electrical losses in the generator. However, the corresponding turbine speed is 1.09 Pu for synchronous generator speed. The DC voltage is regulated at 1200 V, and reactive power is kept at 0 Mvar. At t=0.02 s the positive-sequence voltage suddenly drops to 0.8 Pu causing an oscillation on the DC bus voltage and the DFIG output power. During the voltage sag, the control system regulates DC voltage and reactive power at their set points (1200 V, 0 Mvar). Now the wind farm average DFIG model and Detailed DFIG wind turbine diagram are shown in Figure (2.8 & 2.9) respectively to the illustration of the results. Whereas response of the DFIG regarding voltage at the terminals, active power generated, reactive power requirements and DC capacitor voltage for the SOF-based controller are shown in Fig. 2.10 to 2.17 respectively.

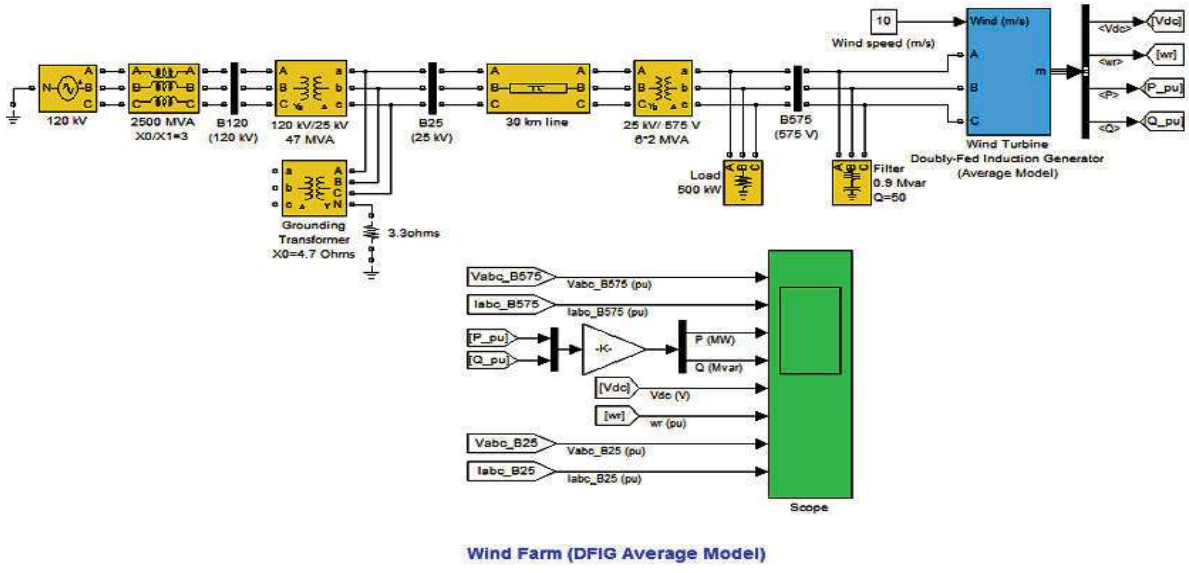

Figure 2.8: Average DFIG model for Wind Farm

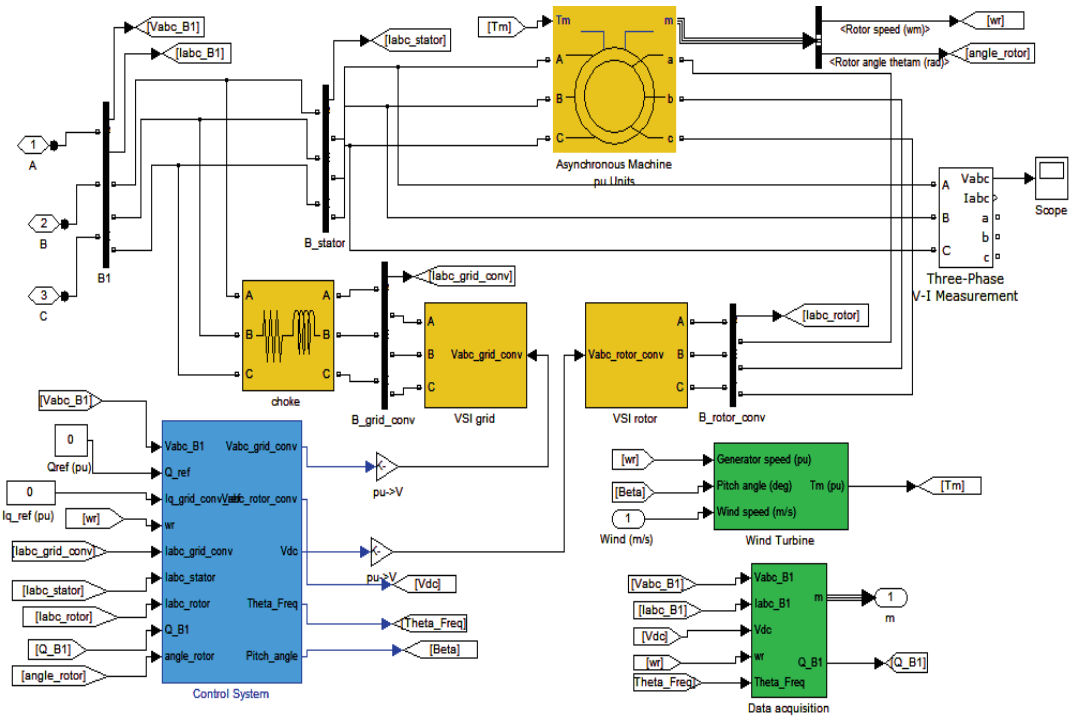

Figure 2.9: Detailed DFIG wind turbine diagram

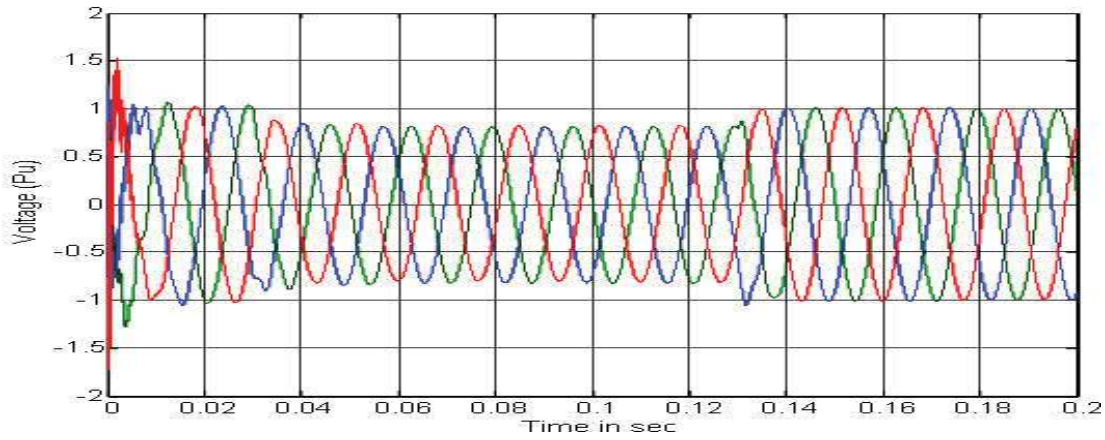

Figure 2.10: Voltages at the DFIG terminals in Pu (SOF-based controller)

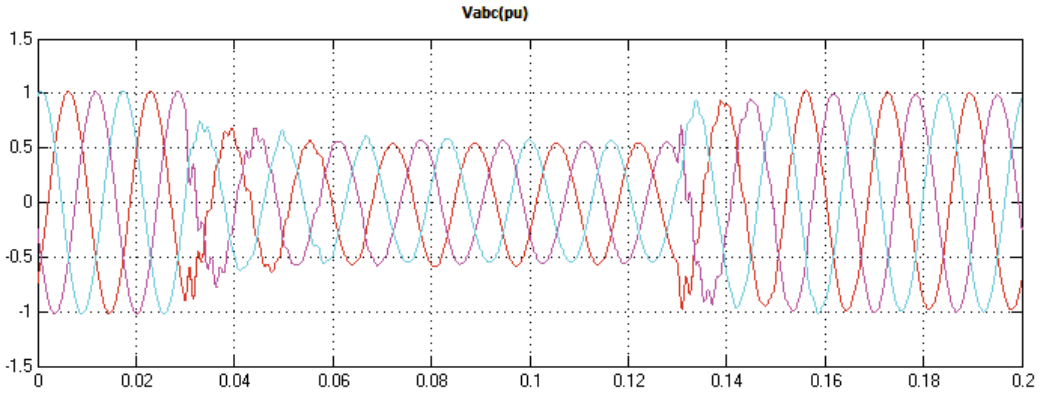

Figure 2.11: Voltages at the DFIG terminals in Pu (supervisory-based controller)

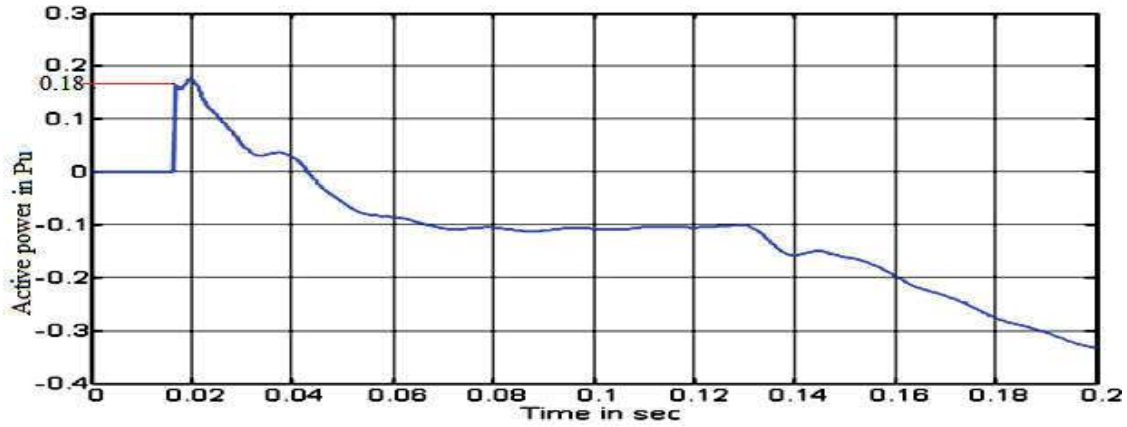

Figure 2.12 Active power delivered of the DFIG in Pu (SOF-based controller)

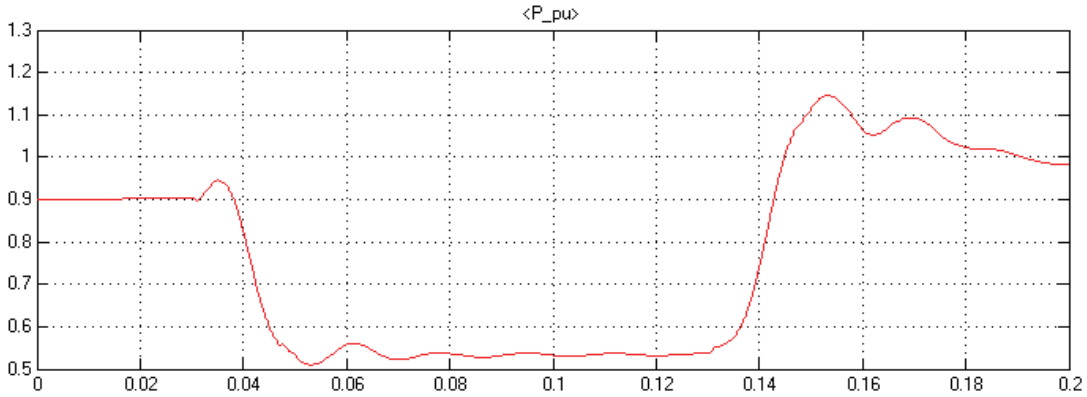

Figure 2.13: Active power given of the DFIG in Pu (supervisory-based controller)

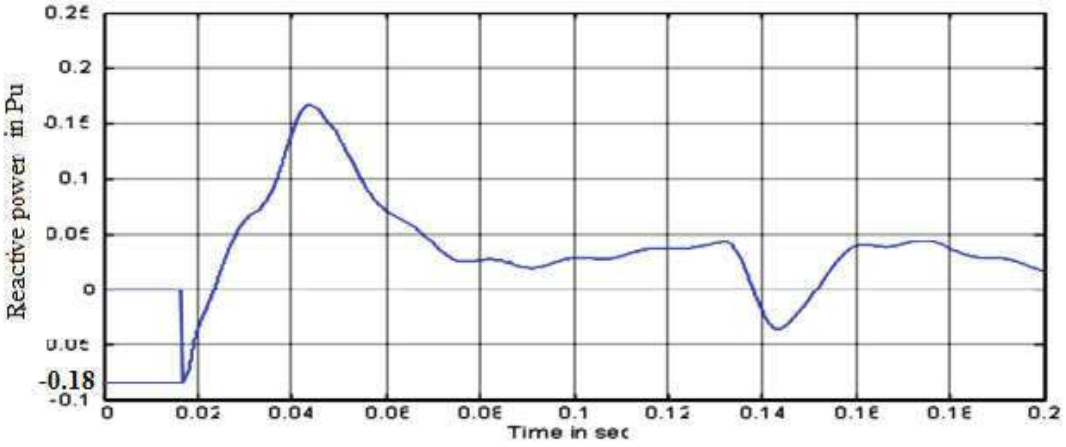

Figure 2.14: Reactive power requirement of the DFIG in Pu (SOF-based controller)

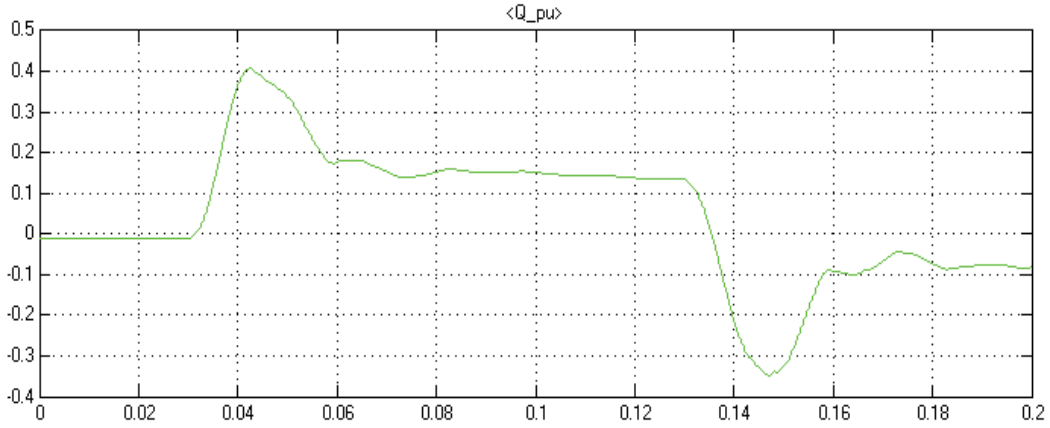

Figure 2.15: Reactive power requirement of the DFIG in Pu (supervisory-based controller)

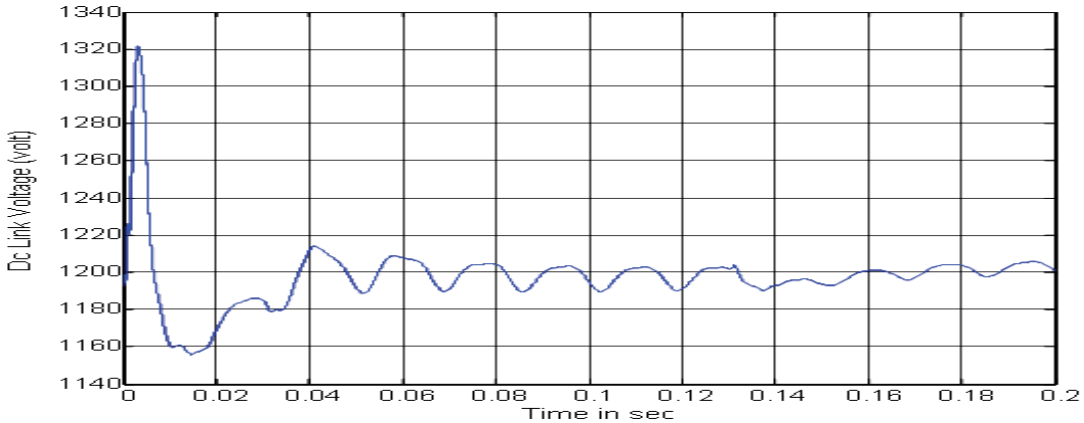

Figure 2.16: DC link voltage at the common link capacitor (SOF-based controller)

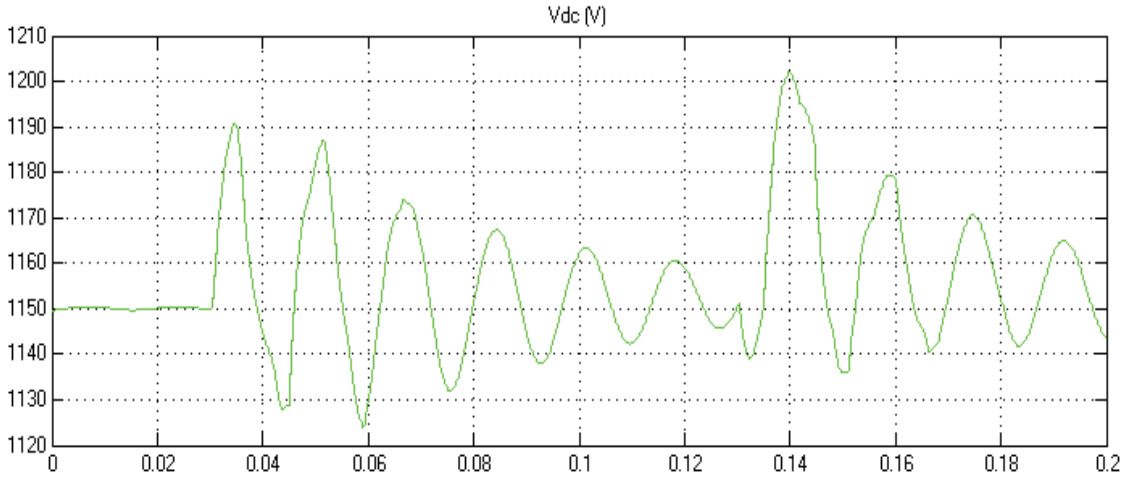

Figure 2.17: DC link voltage at the general coupling capacitor (supervisory-based controller)

Here figure 2.10-2.17 concluded that the response of the DFIG system regarding terminal voltage, active-reactive power, and DC-Link voltage had been improved with a SOF-based controller instead of a supervisory controller.

2.9.2. Response to Supervisory based PID Controller

The response of the supervisory PID designed in [44] on the system under study is as shown in Figure (2.18). Apparently, the open loop system despite being stable has steady-state error of 100%. Further, there is undershoot in the response of the open loop system due to the non-minimum phase nature of the system. Step response of the supervisory-based Conventional PID-controller in [44] is shown in Figure (2.18).

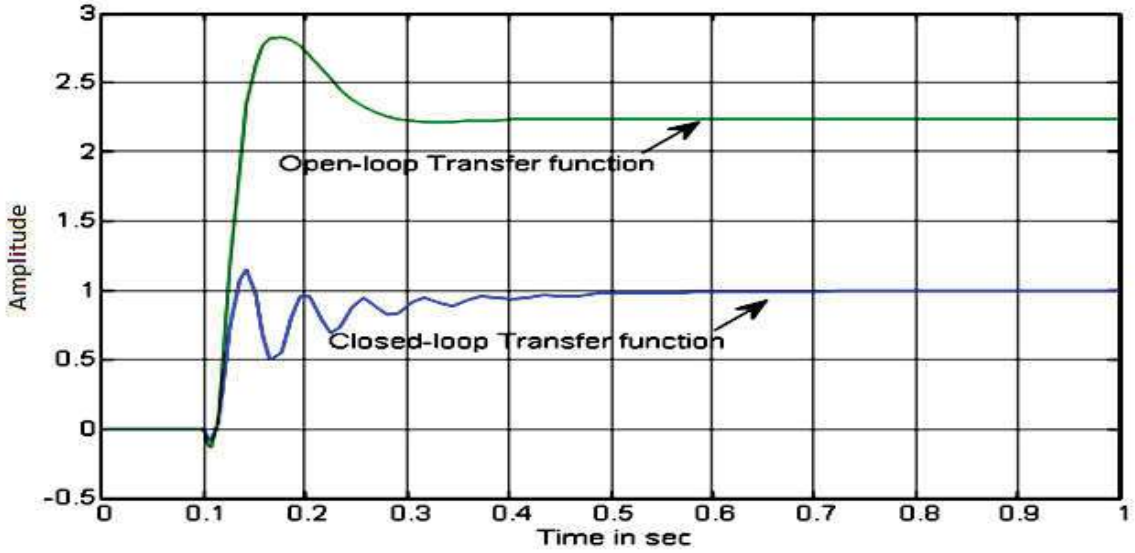

Figure 2.18: Step response of the supervisory-based (Conventional PID controller)

The step response of Figure 2.18 has the following observations as shown in Table (2.3)

Table 2.3: Step response of the supervisory-based (Conventional PID controller) of figure 2.18

Rise Time	Settling Time	Settling Min	Settling Max	Over Shoot	Under Shoot	Peak	Peak Time
0.0152 sec	0.5291sec	0.4933 sec	1.1512 sec	15.1985 %	8.1860 %	1.1512	0.1419 sec

2.9.3 Response of the SOF based Controller

Using PID controller parameters designed in previous Table (2.1) The step response of the system under study for the supervisory reactive power control was studied. The step response of the system is as shown in Figure (2.19). It is evident from a comparison of the results of the PID control in [44] and one reported in this work, that our controller has resulted in suitably damped supervisory control without compromising the speed of response of control loop. Step response of open as well as close loop reduced order system by controller using SOF method is shown in Figure (2.19).

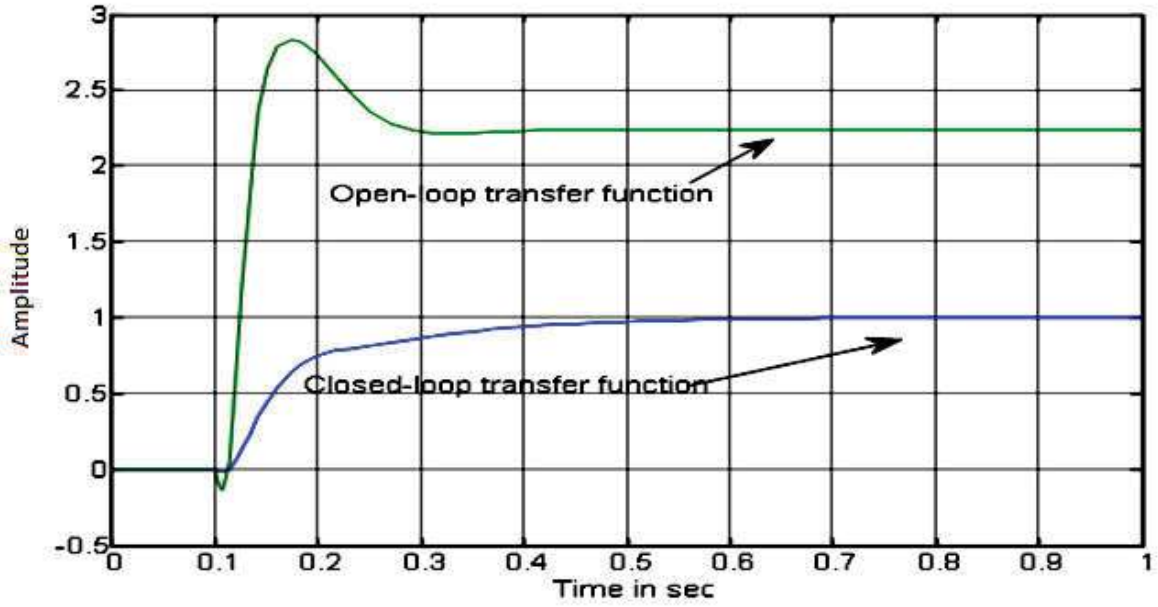

Figure 2.19: Step response of open loop and closed system with SOF based controller

The step response of the system is presented in Figure 9. For the SOF-based controller have the following observations as shown in Table (2.4).

Table 2.4: Step response of figure (2.1 9) with SOF based controller

Rise Time	Settling Time	Settling Min	Settling Max	Over Shoot	Under Shoot	Peak	Peak Time
0.2133 sec	0.5276sec	0.9111 sec	0.9926 sec	0 %	1.5474 %	0.9996	1 sec

2.9.4 Comparison between supervisory and SOF based controller

Comparison of settling time and overshoot are given in Table (2.5). The comparison of the performance parameters for controllers as given in Table (2.4), are concluded as: (i) The designed PI controller can reduce the steady state error to zero as the existing one, (ii) The peak overshoot has been reduced to zero the response is no more underdamped and (iii) The speed of response is almost same as that of the existing controller; or is slightly better. Thus the designed controller in this chapter helps to eliminate the reactive power fluctuations in the DFIG system.

Table 2.5: Comparison of Settling time and Overshoot between Supervisory and SOF controller

Type of controller	Settling time	Overshoot
PID-Supervisory controller	0.5291	15.1985
SOF based controller	0.5276	0

The publications based on this part of the thesis work are as follows:

- **Om Prakash Bharti, R.K Saket, S.K Nagar, "Design of PI controller for doubly fed induction generator using static output feedback**", IEEE 39th National Systems Conference (NSC) Electronic ISBN**: 978-1-4673-6829-2, Noida,** India, 2015.

- **Om Prakash Bharti, R. K. Saket, S. K. Nagar, "Controller Design For DFIG Driven By Variable Speed Wind Turbine Using Static Output Feedback Technique**'', Engineering, Technology & Applied Science Research , ***Vol. 6, No. 4, 2016, 1056-1061. ESCI Journal*** (**Thomson Reuters/Web of Science).**

2.10 Conclusion

The supervisory PID controller even though improves the system response in compare to the open loop system, however, the number of oscillations is not removed entirely. Controller designed using SOF technique not only improves the system response but in addition to reducing the percentage overshoot to zero. Controller using SOF technique shows that the system settles down in smaller time as in the case when supervisory PID controller used. It can be shows

clearly that the settling time is reduced next to three percent approximately as well as the percentage overshoot reduces to zero when controller using SOF method is used in comparison to the supervisory PID controller. Hence, it is concluded that the SOF control technique provides another option for the design of controller to be implemented in DFIG.

In order to observe the performance of the DFIG-based Wind Turbine, along with supervisory and SOF based controllers are designed for the study in this chapter. Hence, next chapter 3 clearly presents the controller design for doubly fed induction generator driven by a variable speed wind turbine using particle swarm optimization technique.